NOAA Technical Memorandum
NWS ER-107

IMPROVING FRESHWATER INFLOWS TO THE NOS CHESAPEAKE BAY OPERATIONAL FORECAST SYSTEM (CBOFS) AND ASSESSING THE IMPACTS ON SALINITY SIMULATIONS

SEANN REED
National Weather Service
Middle-Atlantic River Forecast Center (MARFC)
State College, PA

AMANDA ROBERTS*
Virginia Polytechnic Institute and State University

DUKE N. LE*
Northwest Florida Water Management District

BRECK SULLIVAN*
Chesapeake Research Consortium

* Former summer interns at MARFC supported by NOAAs North Atlantic Regional Team and Chesapeake Bay Office.

Scientific Services Division
Eastern Region Headquarters
Bohemia, New York
November 2020

U.S. DEPARTMENT OF COMMERCE | National Oceanic and Atmospheric Administration | National Weather Service

NOAA TECHNICAL MEMORANDA

National Weather Service, Eastern Region Subseries

The National Weather Service Eastern Region (ER) Subseries provides an informal medium for the documentation and quick dissemination of results not appropriate, or not yet ready for formal publications. The series is used to report on work in progress, to describe technical procedures and practices, or to relate progress to a limited audience. These Technical Memoranda will report on investigations devoted primarily to regional and local problems of interest mainly to ER personnel, and usually will not be widely distributed.

Papers 1 to 22 are in the former series, ESSA Technical Memoranda, Eastern Region Technical Memoranda (ERTM); papers 23 to 37 are in the former series, ESSA Technical Memoranda, Weather Bureau Technical Memoranda (WBTM). Beginning with 38, the papers are now part of the series, NOAA Technical Memoranda NWS.

Papers are available from the National Weather Service Eastern Region, Scientific Services Division, 630 Johnson Avenue, Bohemia, NY, 11716. Beginning with 91, the papers are available at: https://www.weather.gov/erh/TechMemos

ESSA Technical Memoranda

ERTM 1 Local Uses of Vorticity Prognoses in Weather Prediction. Carlos R. Dunn. April 1965.
ERTM 2 Application of the Barotropic Vorticity Prognostic Field to the Surface Forecast Problem. Silvio G. Simplicio. July 1965.
ERTM 3 A Technique for Deriving an Objective Precipitation Forecast Scheme for Columbus, Ohio. Robert Kuessner. September 1965.
ERTM 4 Stepwise Procedures for Developing Objective Aids for Forecasting the Probability of Precipitation. Carlos R. Dunn. November 1965.
ERTM 5 A Comparative Verification of 300 mb. Winds and Temperatures Based on NMC Computer Products Before and After Manual Processing. Silvio G. Simplicio. March 1966.
ERTM 6 Evaluation of OFDEV Technical Note No. 17. Richard M. DeAngelis. March 1966.
ERTM 7 Verification of Probability of Forecasts at Hartford, Connecticut, for the Period 1963-1965. Robert B. Wassall. March 1966.
ERTM 8 Forest-Fire Pollution Episode in West Virginia, November 8-12, 1964. Robert O. Weedfall. April 1966.
ERTM 9 The Utilization of Radar in Meso-Scale Synoptic Analysis and Forecasting. Jerry D. Hill. March 1966.
ERTM 10 Preliminary Evaluation of Probability of Precipitation Experiment. Carlos R. Dunn. May 1966.
ERTM 11 Final Report. A Comparative Verification of 300 mb. Winds and Temperatures Based on NMC Computer Products Before and After Manual Processing. Silvio G.Simplicio. May 1966.
ERTM 12 Summary of Scientific Services Division Development Work in Sub-Synoptic Scale Analysis and Prediction - Fiscal Year 1966. Fred L. Zuckerberg. May 1966.
ERTM 13 A Survey of the Role of Non-Adiabatic Heating and Cooling in Relation of the Development of Mid-Latitude Synoptic Systems. Constantine Zois. July 1966.
ERTM 14 The Forecasting of Extratropical Onshore Gales at the Virginia Capes. Glen V. Sachse. August 1966.
ERTM 15 Solar Radiation and Clover Temperatures. Alex J. Kish. September 1966.
ERTM 16 The Effects of Dams, Reservoirs and Levees on River Forecasting. Richard M. Greening. September 1966.
ERTM 17 Use of Reflectivity Measurements and Reflectivity Profiles for Determining Severe Storms. Robert E. Hamilton. October 1966.
ERTM 18 Procedure for Developing a Nomograph for Use in Forecasting Phenological Events from Growing Degree Days. John C. Purvis and Milton Brown. December 1966.
ERTM 19 Snowfall Statistics for Williamsport, Pa. Jack Hummel. January 1967
ERTM 20 Forecasting Maturity Date of Snap Beans in South Carolina. Alex J. Kish. March 1967.
ERTM 21 New England Coastal Fog. Richard Fay. April 1967.
ERTM 22 Rainfall Probability at Five Stations Near Pickens, South Carolina, 1957-1963. John C. Purvis. April 1967.
WBTM ER 23 A Study of the Effect of Sea Surface Temperature on the Areal Distribution of Radar Detected Precipitation Over the South Carolina Coastal Waters. Edward Paquet. June 1967. (PB-180-612).
WBTM ER 24 An Example of Radar as a Tool in Forecasting Tidal Flooding. Edward P. Johnson. August 1967 (PB-180-613).
WBTM ER 25 Average Mixing Depths and Transport Wind Speeds over Eastern United States in 1965. Marvin E. Miller. August 1967. (PB-180-614).
WBTM ER 26 The Sleet Bright Band. Donald Marier. October 1967. (PB-180-615).
WBTM ER 27 A Study of Areas of Maximum Echo Tops in the Washington, D.C. Area During the Spring and Fall Months. Marie D. Fellechner April 1968. (PB-179-339).
WBTM ER 28 Washington Metropolitan Area Precipitation and Temperature Patterns. C.A. Woollum and N.L. Canfield. June 1968. (PB-179-340).
WBTM ER 29 Climatological Regime of Rainfall Associated with Hurricanes after Landfall. Robert W. Schoner. June 1968. (PB-179-341).
WBTM ER 30 Monthly Precipitation - Amount Probabilities for Selected Stations in Virginia. M.H. Bailey. June 1968. (PB-179-342).
WBTM ER 31 A Study of the Areal Distribution of Radar Detected Precipitation at Charleston, S.C. S.K. Parrish and M.A. Lopez. October 1968. (PB-180-480).
WBTM ER 32 The Meteorological and Hydrological Aspects of the May 1968 New Jersey Floods. Albert S. Kachic and William Long. February 1969. (Revised July 1970). (PB-194-222).
WBTM ER 33 A Climatology of Weather that Affects Prescribed Burning Operations at Columbia, South Carolina. S.E. Wasserman and J.D. Kanupp. December 1968. (COM-71-00194).
WBTM ER 34 A Review of Use of Radar in Detection of Tornadoes and Hail. R.E. Hamilton. December 1969. (PB-188-315).
WBTM ER 35 Objective Forecasts of Precipitation Using PE Model Output. Stanley E. Wasserman. July 1970. (PB-193-378).
WBTM ER 36 Summary of Radar Echoes in 1967 Near Buffalo, N.Y. Richard K. Sheffield. September 1970. (COM-71-00310).
WBTM ER 37 Objective Mesoscale Temperature Forecasts. Joseph P. Sobel. September 1970. (COM-71-0074).

NOAA Technical Memoranda NWS

NWS ER 38 Use of Primitive Equation Model Output to Forecast Winter Precipitation in the Northeast Coastal Sections of the United States. Stanley E. Wasserman and Harvey Rosenblum. December 1970. (COM-71-00138).
NWS ER 39 A Preliminary Climatology of Air Quality in Ohio. Marvin E. Miller. January 1971. (COM-71-00204).
NWS ER 40 Use of Detailed Radar Intensity Data in Mesoscale Surface Analysis. Robert E. Hamilton. March 1971. (COM-71-00573).
NWS ER 41 A Relationship Between Snow Accumulation and Snow Intensity as Determined from Visibility. Stanley E. Wasserman and Daniel J. Monte. (COM-71-00763). January 1971.
NWS ER 42 A Case Study of Radar Determined Rainfall as Compared to Rain Gage Measurements. Martin Ross. July 1971. (COM-71-00897).
NWS ER 43 Snow Squalls in the Lee of Lake Erie and Lake Ontario. Jerry D. Hill. August 1971. (COM-72-00959).
NWS ER 44 Forecasting Precipitation Type at Greer, South Carolina. John C. Purvis. December 1971. (COM-72-10332).
NWS ER 45 Forecasting Type of Precipitation. Stanley E. Wasserman. January 1972. (COM-72-10316).

(CONTINUED ON INSIDE REAR COVER)

NOAA Technical Memorandum NWS ER-107

IMPROVING FRESHWATER INFLOWS TO THE NOS CHESAPEAKE BAY OPERATIONAL FORECAST SYSTEM (CBOFS) AND ASSESSING THE IMPACTS ON SALINITY SIMULATIONS

SEANN REED
National Weather Service
Middle-Atlantic River Forecast Center (MARFC)
State College, PA

AMANDA ROBERTS*
Virginia Polytechnic Institute and State University

DUKE N. LE*
Northwest Florida Water Management District

BRECK SULLIVAN*
Chesapeake Research Consortium

* Former summer interns at MARFC supported by NOAAs North Atlantic Regional Team and Chesapeake Bay Office.

Scientific Services Division
Eastern Region Headquarters
Bohemia, New York
November 2020

Table of Contents

Abstract

The Chesapeake Bay Operational Forecast System (CBOFS) is a 3D hydrodynamic model which generates 48-hour forecasts of water level, currents, temperatures and salinity throughout the Chesapeake Bay. A limitation of the current CBOFS is that it does not use forecast information available from modern river forecast models. Currently, river inflows are derived by persisting the flow observations from U.S. geological survey stream gages, and the gages used measure runoff from only 79% of the Bay watershed area. In this study, we investigate the potential benefits of using hydrologic modeling to provide CBOFS with more accurate estimates of river inflows. Specifically, we study the impact of using more detailed and accurate streamflow inputs on the model's ability to predict salinity. In our simulation experiments, we increased the number of river inflow nodes from 13 to 60. Salinity is studied because of its sensitivity to freshwater inflows and its importance to marine life in the Bay. As expected, adding more freshwater to the model does reduce high salinity bias from CBOFS that has been noted in earlier studies; however, some bias still remains. The spatial pattern of salinity simulation improvements are also consistent with expectations. That is, more improvement is seen in shallow waters closer to the added river inputs. To expedite this study, we used the Research Distributed Hydrologic Model (RDHM) to simulate flows on small rivers. Moving forward, the more feasible path for operational implementation on small rivers is to use flows from NOAAs National Water Model.

Introduction

NOAAs National Ocean Service runs Operational Forecast Systems (OFSs) for critical ports and estuaries in the United States. Operational Forecast Systems provide useful information about water conditions for many users such as ship navigators, recreational boaters, fishermen, fisheries managers, public health officials, hazardous material response teams, search and rescue personnel, and others. The Chesapeake Bay OFS (CBOFS) generates 48-hour forecasts for water level, currents, temperatures and salinity throughout the Chesapeake Bay (NOAA National Ocean Service, 2011). Here we study how the hydrodynamic model underlying CBOFS can be improved by improving the accuracy of hydrologic inflows from the surrounding rivers and streams. Specifically, we analyze the impacts of freshwater inflow improvements on salinity simulations.

Why is this important?

There are known limitations with respect to river inflows in the current CBOFS implementation. First, CBOFS only explicitly accounts for 13 river inflows into the Bay using data from U.S. Geological Survey (USGS) stream gages (Figure 1). These 13 river inflows represent only about 79% of the Chesapeake Bay drainage area. Second, river inflows to CBOFS for the 48-hour forecast period are estimated by simply persisting observed flow data. This does not accurately reflect the impacts of rising flows during storm events. At this time, several available hydrologic models are capable of simulating flows from all rivers draining to the Bay. These models can produce more accurate inflows by explicitly accounting for more of the watershed drainage area. In addition, use of forecast information from hydrologic models will improve upon persistence estimates at inflow locations.

We focus on salinity because our hypothesis is that improving the river inflow accuracy will have a relatively large impact on the CBOFS salinity forecasts compared to other variables such as currents. Also, positive salinity bias is a known issue in the operational CBOFS model (Lanerolle et al., 2016). We investigate whether adding inflow nodes to the operational CBOFS model might have dramatic local impacts on salinity forecasts in smaller river estuaries within the Bay.

Salinity has important impacts on the Bay ecosystem. Salinity affects the health and spatial distribution of numerous Chesapeake Bay species such as fish, oysters, and blue crabs. Salinity also influences biological process rates which can affect processes important to humans such as harmful algal blooms and oyster growth.

NOAA already uses salinity and temperature forecasts from CBOFS to make real-time predictions about the prevalence and location of stinging sea nettles and harmful Vibrio bacteria (NOAA OPC, 2019; NCCOS 2020). Li et al. (2001) describe the scientific foundation for the sea nettle forecasting system while Lanerolle et al. (2016) do the same for the Vibrio forecasting. In both cases, an empirical relationship translates temperature and salinity outputs from CBOFS

into forecast variables of interest: sea nettle encounter probabilities and Vibrio concentrations. Improved river inflows to CBOFS should improve these sea nettle and Vibrio forecasts.

What is unique about this study?

Like the operational CBOFS implementation, academic and regulatory hydrodynamic model implementations in the Chesapeake Bay most often do not explicitly account for inflows from smaller watersheds (Xu et al., 2012; Feng et al., 2015; Cerco et al., 2010). In some cases, this is because the main study foci were on the deeper parts of the bay. An exception is the work of Ye et al. (2018) which accounts for more of the smaller tributaries. They noted that adding the smaller tributaries into their modeling did improve the accuracy of their results; however, they did not elaborate on details. Our study more explicitly addresses the impacts of accounting for the smaller tributaries. In addition, we use hydrodynamic and hydrologic models which are already used in NOS and NWS operations. Therefore, the transition from research-to-operations should be relatively easy.

This study was completed through a unique inter-office collaboration within NOAA. NOAA's North Atlantic Regional Team (NART) funded three summer internships for undergraduates while the NOAA Chesapeake Bay Office and Chesapeake Research Consortium facilitated these internships. NOAAs National Weather Service (NWS) Middle Atlantic River Forecast Center (MARFC) hosted the three students and guided the research with assistance from modelers at the NOS Center for Operational Products and Services (COOPS) and the Coast Survey Development Laboratory (CSDL).

How does this study contribute to the NOAA goals?

The goals of this study are in line with the NOAA Water Initiative Vision and Five-Year Plan (NOAA, 2016), which includes goals to advance water quality forecasting in riverine and estuarine environments and to create new capabilities to leverage water quality predictions for ecological applications. This research tackles only a small piece of this bigger picture, but did so using minimal resources. The hydrologic model used in this study is a regional model selected so that it could be run at the MARFC to complete the project; however, the same methods could be used to pass outputs from NOAAs National Water Model (NWM, 2020) to CBOFS. The NWM is a major component of the NOAA Water Initiative.

Our outcomes do the following: (1) demonstrate that there is value in substantially increasing the number of river inflow nodes to CBOFS, (2) demonstrate that CBOFS remains computationally stable with this increase in river nodes, and (3) provide configuration details that could be used to modify the current operational CBOFS model.

Methods

Hydrodynamic Model

Lanerolle et al. (2011) describe the development and skill assessment of the model that underlies the current Chesapeake Bay Operational Forecast System, CBOFS2. While the first CBOFS was based on a 2-dimensional model and only provided information on water levels and depth-averaged currents, CBOFS2 is a 3-dimensional model and provides information on water levels, currents, temperature, and salinity. CBOFS2 is an implementation of Rutgers University's Regional Ocean Model System.

For our baseline simulation, we ran CBOFS2 using a model configuration and forcing files provided by Lyon Lanerolle (personal communication, 2016). The baseline simulation input files are identical to those Lanerolle et al. (2011) used for their 'synoptic simulation.' For meteorological fluxes, Lanerolle et al. (2011) combined gridded data from the North American Regional Reanalysis (Mesinger et al., 2006) with local gage information. For the open ocean boundary conditions they used monthly climatology data from the World Ocean Atlas 2001 (Conkright et al., 2002). The only difference in our calculations for this baseline run is that we recompiled the executable on a different High Performance Computing development platform. The original simulations were run on NOAAs 'Jet' machine while our simulations were run on NOAAs 'Theia' platform.

Figure 1 shows the CBOFS2 model mesh along with the locations of the river input nodes used by Lanerolle et al. (2011). The flows estimated at a given node are sometimes estimated from more than one upstream US Geological Survey gage as specified in Table 1. These are also the gages used for operational CBOFS2 runs as of October 2020.

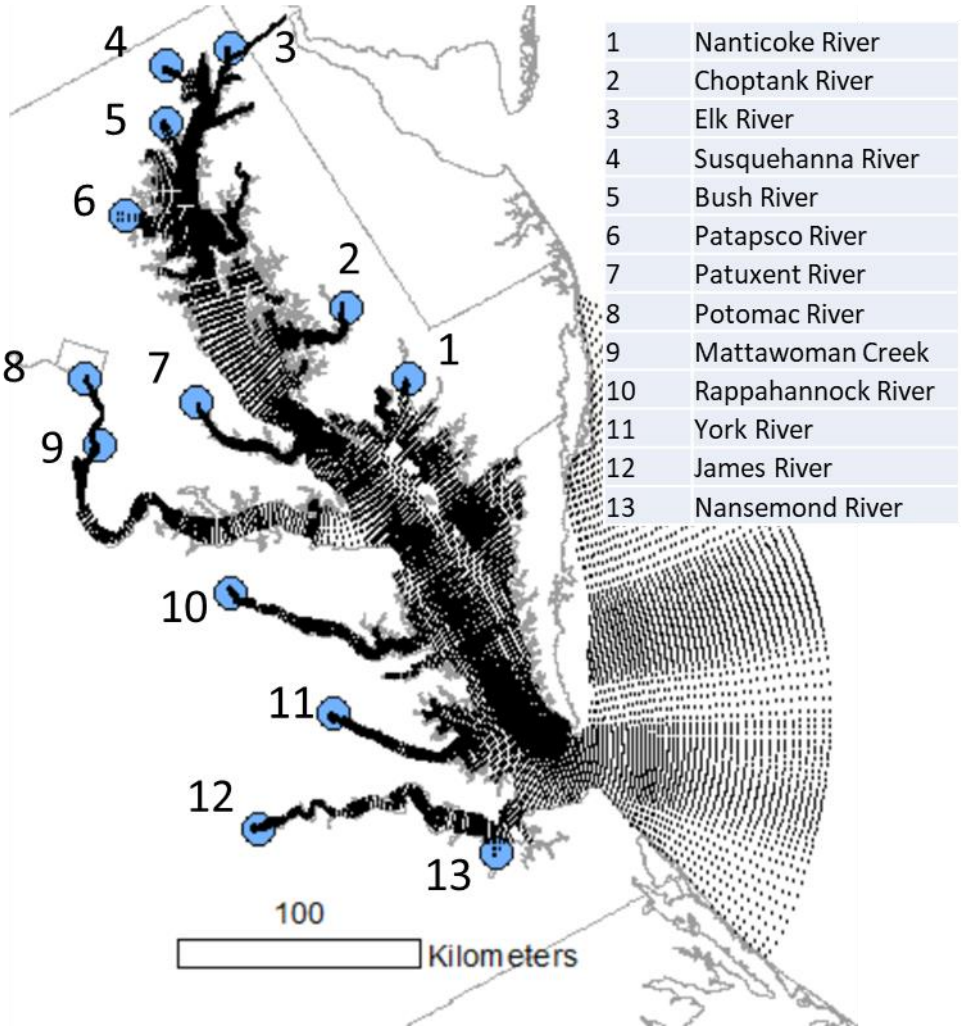

Figure 1. CBOFS2 model mesh and river inflow node locations for operational runs.

Table 1. USGS Flow Observation Stations used to Derive CBOFS2 inflows.

	CBOFS Input Node	USGS ID	Name	Drainage Area (mi2)
1	Nanticoke River	Unknown		
2	Choptank River			
		1491000	Choptank R near Greensboro MD	113
		1491500	Tuckahoe Cr near Ruthsburg MD	85.2
3	Elk Creek			
		1495000	Big Elk Cr at Elk Mills MD	51.6
4	Susquehanna River			
		1578310	Susquehanna R at Conowingo MD	27100
		1580520	Deer Cr near Darlington MD	164
5	Bush River			
		1581757	Otter Point Creek near Edgewood MD	55.6
6	Patapsco River			
		1589352	Gwynns Falls at Wash Blvd at Balt	65.9
7	Patuxent River			
		1594440	Patuxent R near Bowie MD	348
		1594526	W Branch at Upper Marlboro MD	89.7
8	Potomac River			
		1646500	Potomac R near Little Falls	11560
9	Mattawoman Creek	1658000	Mattawoman Cr nr Pomonkey MD	54.8
10	Rappahannock			
		1668000	Rappahannock R near Fredericksburg	1595
11	York River			
		1673000	Pamunkey R near Hanover VA	1078
		1674500	Mattaponi R near Beulahville VA	603
12	James River			
		2037500	James R near Richmond VA	6753
		2041650	Appomatox River at Matoaca VA	1342
13	Nansemond River			
		2049500	Blackwater R near Franklin VA	613

An important consideration when passing flows from a river outside of the model to CBOFS2 nodes is to ensure that there is no numerical instability due to rapidly changing conditions at the boundary nodes. To maintain stability, we followed the methods used by Lanerolle et al. (2011). Large river flows are distributed laterally across several CBOFS2 boundary nodes in proportion to the normal water depth. In addition, a pre-defined vertical velocity distribution is prescribed as a function of depth at the boundary nodes to approximately account for the effects of bottom friction. Figure 2 conceptually illustrates this lateral and vertical distribution of flows at the upstream end of the James River, VA.

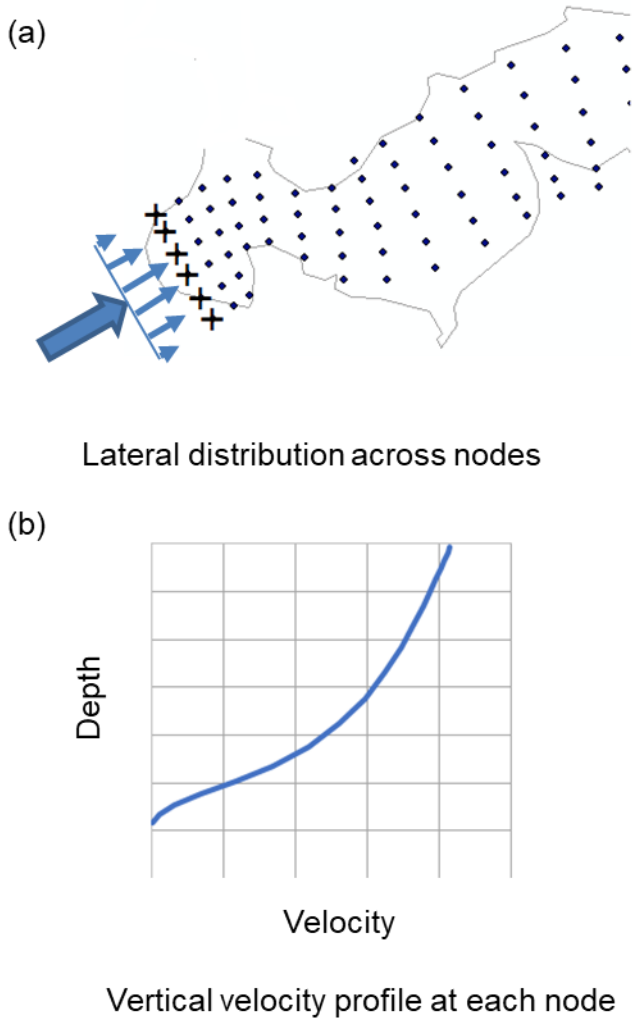

Figure 2. (a) Example of lateral flow distribution across nodes for the James River CBOFS2 inflow, (b) default vertical velocity profile at inflow nodes.

Watershed Model

Using a watershed model with more complete coverage of the Chesapeake Bay Drainage area is a primary component of this study. The dark green shaded area in Figure 3a shows the watershed drainage areas captured by the USGS gages listed in Table 1. CBOFS2 does not explicitly account for the light green and yellow shaded areas in Figure 3a within the Chesapeake portion of the map. For the rivers included in the operational CBOFS2, USGS flows are adjusted to account for the intervening drainage areas between the gage locations and the 13 Bay input nodes shown in Figure 1 (also as black dots in Figure 3b). In this study, we experimented with adding additional rivers and connections to CBOFS2. Initially we took a cautious approach and only increased the number of rivers represented from 13 to 22. Because this increase caused no model stability problems, we then proceeded to increase the number of rivers to 60 and these are

the results reported here. The 60 rivers includes all rivers within the Chesapeake Watershed with a drainage area of at least 50 mi^2. Figure 3b highlights basins added.

We refer to model runs with the 13 original input nodes as Scenario 1 (S1) and the model runs with 60 river inputs as Scenario 2 (S2). Table 2 summarizes percentage of the Chesapeake Watershed area observed and accounted for in each scenario. In the simulation mode used here, both scenarios use observed flows where available. In Scenario 1, drainage area coefficients are computed to account for the locations of the stream gages as described by Xu et al. (2012), and flows are scaled by these amounts to represent the water contributions downstream of these gages (hence the increase from 79% observed to 85% observed and modeled). In Scenario 2, 10% additional area is accounted for by the 47 additional input nodes for small rivers, making the total area observed and modeled 95%.

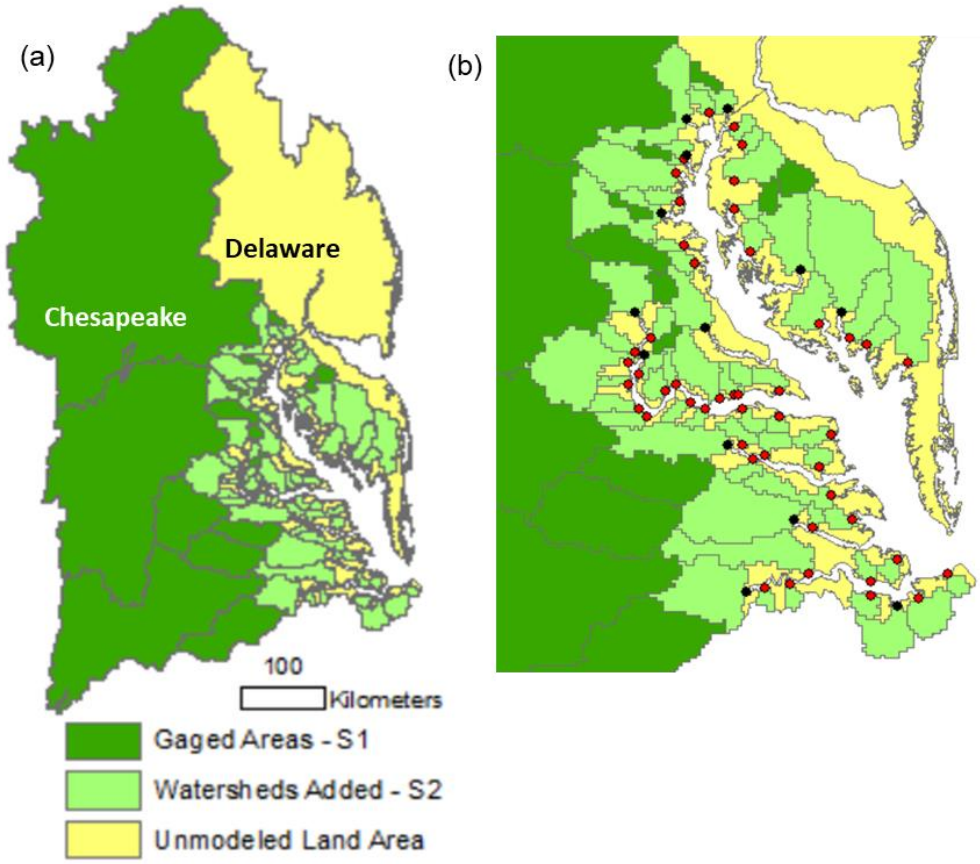

Figure 3. Modeled areas for Scenarios 1 and 2: (a) middle Atlantic domain, and (b) zoomed to watersheds added for Scenario 2; black dots are the original input nodes and red dots are added input nodes.

Table 2. Percent of drainage area observed and modeled in simulation studies.

Scenario	% area observed	% area observed + modeled
S1	79	85
S2	79	95

To simulate outflows for the ungaged sub-watersheds in Scenario 2, we used the Hydrology Laboratory's Research Distributed Hydrologic Modeling System (HL-RDHM) (Koren et al., 2004). In our implementation, HL-RDHM is applied at a 2-km grid cell resolution to the entire Chesapeake drainage basin. Figure 4 shows the river network formed by inter-connected 2-km grid cells in the model. Our HL-RDHM implementation uses the gridded Snow-17, the gridded Sacramento Soil Moisture Accounting Model with Heat Transfer (SAC-HT), and kinematic wave routing as described by Koren et al. (2007). The forcings used for snow melt and rainfall-runoff modeling include gridded hourly precipitation, gridded hourly temperature, and gridded monthly evapotranspiration demand estimates. The precipitation grids were from MARFCs multi-sensor precipitation analyses which blend radar estimates with quality controlled rain-gage estimates to yield 'best estimate' grids. The hourly temperature grids were created by blending hourly and daily point temperature observation data to generate hourly grids. The gridded evapotranspiration demand fields provided as default inputs to HL-RDHM were developed based on remotely sensed vegetation fields, select calibrated watersheds, and monthly climatological data.

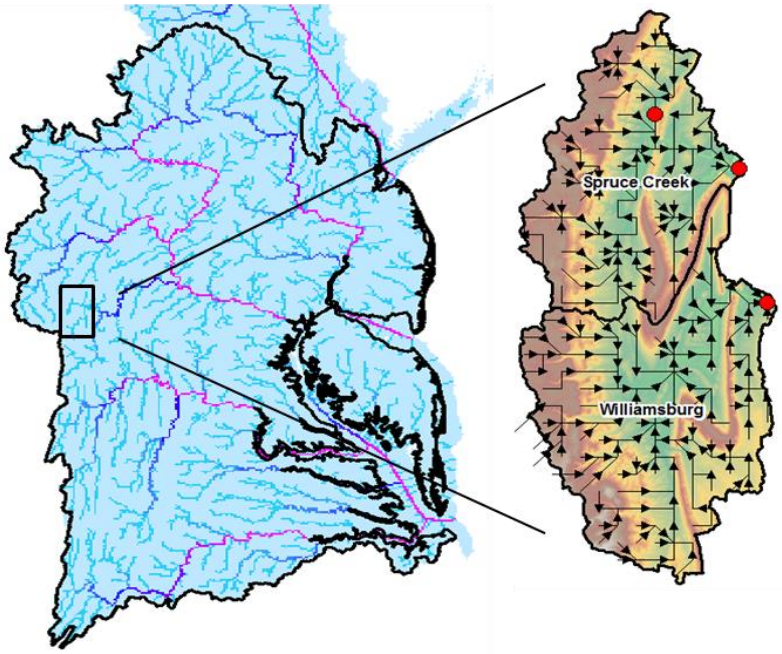

Figure 4. HL-RDHM modeled rivers based on 2-km grid cells with a magnified area showing the cell-to-cell network in two headwater basins.

No comprehensive calibration was done for these HL-RDHM hydrologic model simulations. Parameters for the snow, rainfall-runoff, and routing calculations are *a priori* parameters derived from physical data sets (Koren et al., 2007; Mizukami and Koren, 2008) or default values for a region. Approximate adjustments to the monthly evapotranspiration demand grids were applied to match experience with calibrating a few small basins in the region.

Some of the 60 river simulation points shown in Figure 3 are downstream of the USGS gages used in the operational CBOFS2 runs. For any of the rivers containing a gage in Table 1, the observed data is used for the gaged portion of the basin and the HL-RDHM modeled flow is added for the ungaged portion of the basin. This limits hydrologic simulation errors to only the ungaged areas, shaded light green in Figure 3.

We selected the HL-RDHM software for use in this study because it has performed well in model inter-comparisons (Reed et al., 2004; Smith et al., 2012), it is relatively easy to re-run simulations for long periods of time, and the software is already running in real-time at the Middle Atlantic River Forecast Center. While we leveraged HL-RDHM to facilitate this study, no more development work is being done on HL-RDHM and much more effort at the National level goes into building the National Water Model (NWM) for real-time forecasts (OWP, 2020). While it was infeasible to use the NWM in this study, we expect that the NWM will be a more practical platform to simulate river flows from ungaged basins in future applications. The simple methods to pass river flows to CBOFS2 used here are applicable to either HL-RDHM or NWM output. The same CBOFS2 configuration files could be used in either case.

Study Design

In our results, we show outputs from two model scenarios:

- Scenario 1 (S1): The baseline case with 13 rivers represented.
- Scenario 2 (S2): The enhanced scenario with 60 rivers represented.

Each scenario was analyzed for two different time periods. The first time period was the same as that used by Lanerolle et al. (2011), spanning June 2003 to September 2005; however, we discarded the first six months of output from our analysis to avoid model spin-up errors. For additional validation, we selected a more recent period from January 1, 2016 to December 31, 2016. For this period, archived forcings were provided by NOS COOPs from their operational database. No model spin-up was required for the 2016 period because initial conditions were taken from saved operational model states.

Validation

We validated salinity simulations from CBOFS2 against salinity observations from the Chesapeake Bay Programs Tidal Water Quality Monitoring program (CBP, 2020). For the time periods in this study, we downloaded data for 64 sampling locations that correspond to CBOFS2 output locations and have valid data. The salinity observations are discrete observations taken by

boat, once or twice per month at each site. At each site, observations are available at multiple depths, 1-m intervals from the water surface to the Bay floor. Figure 5 shows the identifiers and locations for the observations.

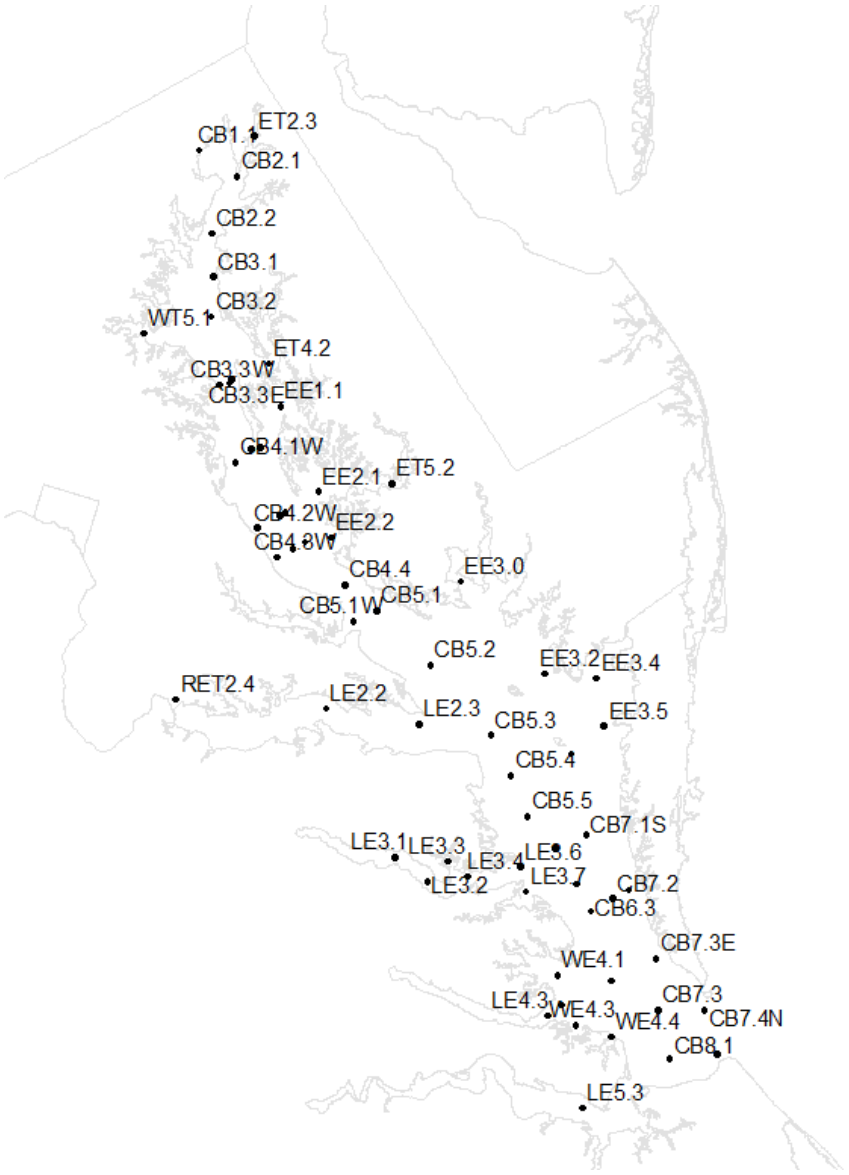

Figure 5. Chesapeake Bay Program monitoring stations used for validation.

We evaluate the salinity simulations from Scenarios 1 and 2 using three main methods for each location: (1) we compute and map summary statistics comparing simulated and observed salinities (at the 1-m depth and for the profile average), (2) plot and compare simulated and observed salinity profiles for individual locations, and (3) plot time series of 1-m simulated and observed salinity to observe temporal trends. To facilitate these comparisons, simulated salinity estimates output from CBOFS2 are interpolated vertically to the standard 1-m interval observation depths.

Many of the statistic and graphics presented here were generated using Python scripts developed for this project. These scripts leverage the Matplotlib and GeoPandas libraries.

Results and Discussion

Figures 6a and 6b show the Scenario 1 profile mean error in the salinity forecasts for all sampling locations and the 2004 and 2016 study periods respectively. To compute 'Profile Mean Error', the error is averaged over all observed depths and all the sampling times during the study period. During both study periods, the Scenario 1 salinity is too high over most of the Bay, which is consistent with the observations of Lanerolle et al. (2011). This positive error is more pronounced and consistent across all locations during the 2016 period compared to 2004. Figures 6c and 6d show the profile mean salinity error predicted by Scenario 2. Not surprisingly Scenario 2 mean errors are lower during both periods due to the additional freshwater inflows to the model. For Scenario 1 the average mean error over all locations is 0.96 psu for 2004 and 3.8 psu for 2016 (where psu is practical salinity unit). For Scenario 2, these values drop to 0.47 psu for 2004 and 2.9 psu for 2016. Figures 6e and 6f show the change in salinity between the two scenarios (Scenario 2 – Scenario 1). In Figures 6e and 6f, all plotted values are negative, indicating that salinities were reduced in Scenario 2 across the board.

Still looking at average statistics for the whole profile, Figures 7a and 7b show the Root Mean Squared Error (RMSE) for Scenario 1 and Scenario 2 in 2016. Figure 7c shows the Scenario 1 RMSE minus Scenario 2 RMSE. Values in Figure 7c are all positive except for one location, indicating that the errors are higher in Scenario 1 compared to Scenario 2. This shows that adding more accurate freshwater inflows increases salinity simulation accuracy across the Bay. Figure 7d highlights the stations where the five largest improvements in RMSE are observed: EE3.0, ET5.2, LE3.3, WE4.4, and LE5.3. These locations are more strongly influenced by the freshwater inflows from the relatively smaller tributaries which are not accounted for in Scenario 1. Figure 7d also includes the one location, CB1.1, where S1-S2 salinity was slightly negative, indicating a worse simulation. This will be explained in the analysis below.

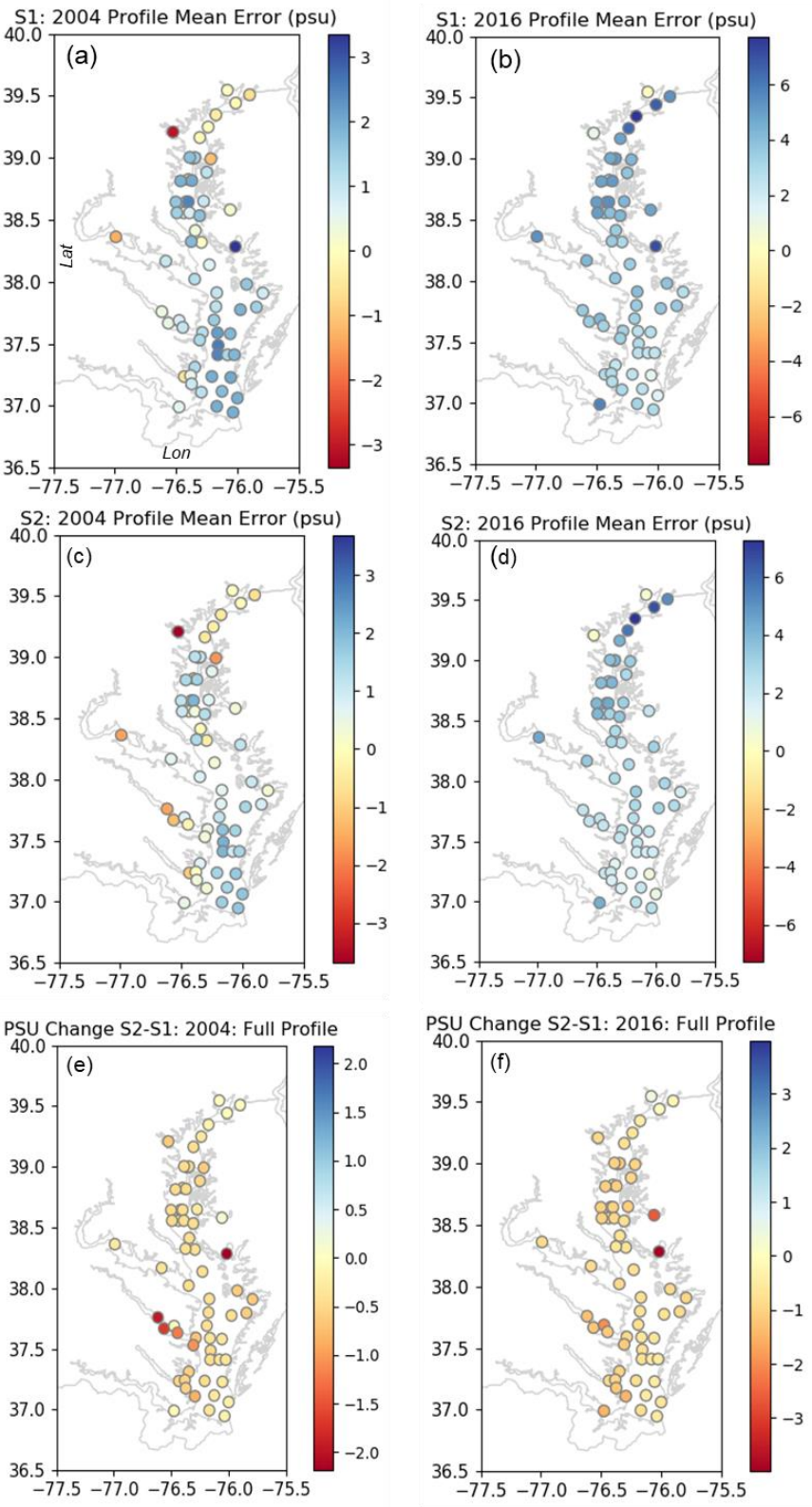

Figure 6. Mean profile error computed over all sampling depths and observation times for each location: (a) Scenario 1 2004, (b) Scenario 1 2016, (c) Scenario 2 2004, (d) Scenario 2 2016, (e) Scenario 2 – Scenario 1 2004 (negative values show decreases in predicted salinity), and (f) Scenario 2 – Scenario 1 2016.

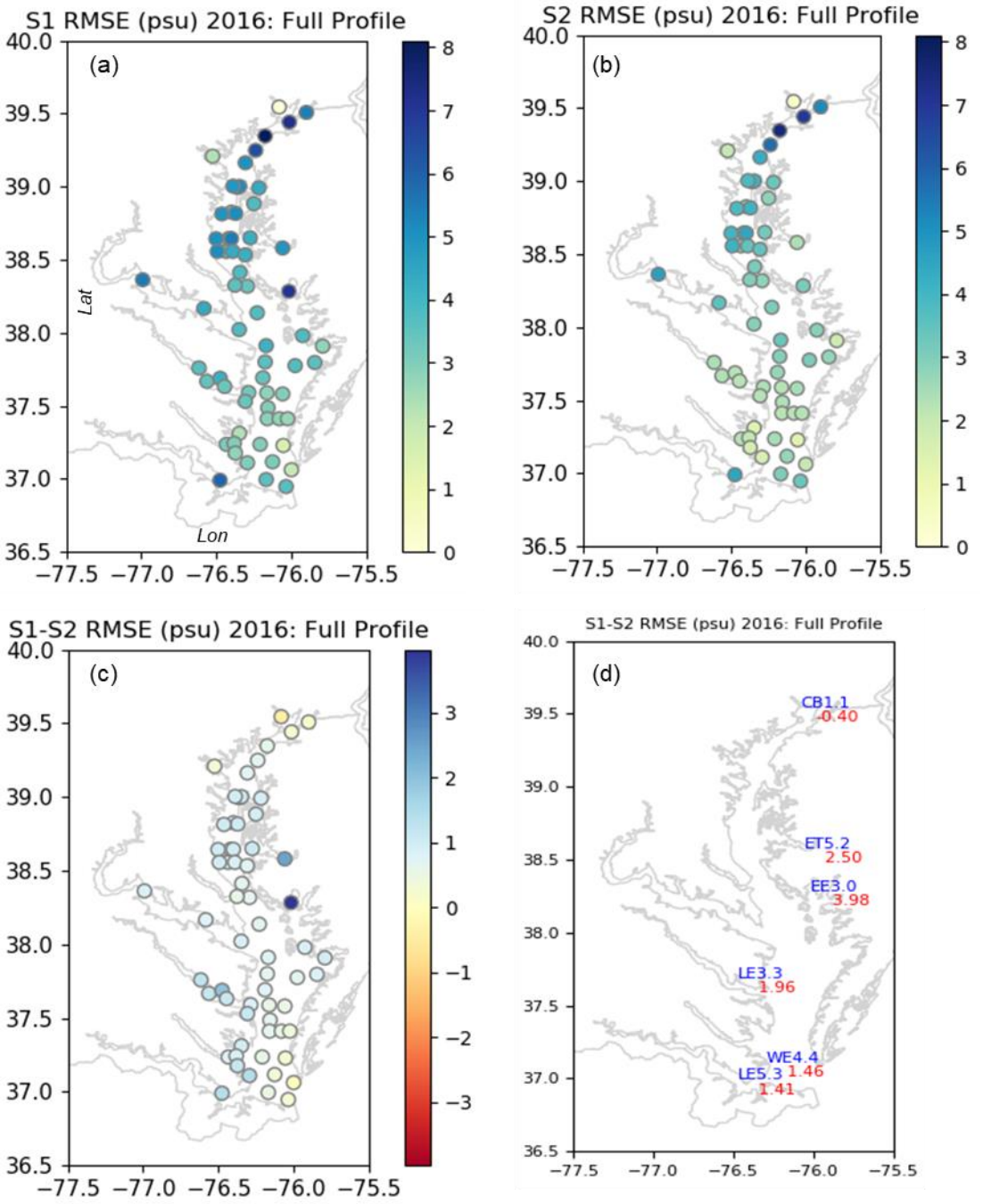

Figure 7. Profile Root Mean Squared Error (RMSE) computed over all sampling depths and all observation times at each location: (a) Scenario 1 2016, (b) Scenario 2 2016, (c) Scenario 1 – Scenario 2 : positive numbers mean improvement in Scenario 2, and (d) 5 locations with the largest RMSE improvement and one location with negative improvement.

Table 3. Summary statistics for the 2016 period averaged across the whole profile and all observation times. ME=mean error (a.k.a. bias); MAE=mean absolute error; RMSE=root mean squared error.

	ID	S1 MAE	S1 ME	S1 RMSE	S2 MAE	S2 ME	S2 RMSE	S2-S1 ME	S1-S2 RMSE
1	CB1.1	0.03	-0.02	0.03	0.39	0.39	0.44	0.41	-0.40
2	CB2.1	6.70	6.65	7.22	6.62	6.62	6.95	-0.03	0.27
3	CB2.2	7.76	7.74	8.11	7.28	7.28	7.51	-0.46	0.60
4	CB3.1	6.36	6.36	6.44	5.69	5.69	5.74	-0.67	0.70
5	CB3.2	4.90	4.90	5.03	4.16	4.15	4.28	-0.74	0.74
6	CB3.3C	3.84	3.83	4.11	3.08	3.05	3.38	-0.78	0.74
7	CB3.3E	5.08	5.08	5.16	4.03	4.01	4.12	-1.07	1.04
8	CB3.3W	4.71	4.70	4.87	3.73	3.67	3.89	-1.03	0.98
9	CB4.1C	3.22	3.16	3.53	2.58	2.43	2.88	-0.73	0.66
10	CB4.1E	5.12	5.12	5.15	4.07	4.07	4.10	-1.05	1.04
11	CB4.1W	4.87	4.87	4.92	3.82	3.82	3.90	-1.05	1.03
12	CB4.2C	4.04	4.04	4.21	3.29	3.29	3.48	-0.75	0.74
13	CB4.2E	5.44	5.44	5.48	4.43	4.43	4.48	-1.01	1.00
14	CB4.2W	5.02	5.02	5.06	4.00	4.00	4.05	-1.03	1.01
15	CB4.3C	3.56	3.56	3.80	2.85	2.84	3.10	-0.72	0.70
16	CB4.3E	3.99	3.98	4.36	3.13	3.06	3.48	-0.93	0.87
17	CB4.3W	5.03	5.03	5.13	4.02	4.02	4.14	-1.01	0.99
18	CB4.4	3.54	3.54	3.81	2.85	2.83	3.13	-0.71	0.68
19	CB5.1	3.13	3.03	3.45	2.49	2.32	2.80	-0.71	0.65
20	CB5.1W	3.52	3.52	3.57	2.93	2.93	2.98	-0.60	0.59
21	CB5.2	3.51	3.48	3.75	2.81	2.76	3.05	-0.73	0.70
22	CB5.3	4.04	4.04	4.17	3.28	3.28	3.42	-0.76	0.75
23	CB5.4	3.53	3.53	3.64	2.84	2.84	2.96	-0.69	0.68
24	CB5.5	3.34	3.33	3.47	2.60	2.55	2.72	-0.78	0.75
25	CB6.1	2.64	2.62	2.84	2.07	2.01	2.28	-0.61	0.56
26	CB6.2	2.86	2.84	3.00	2.17	2.11	2.34	-0.73	0.66
27	CB6.3	2.67	2.61	2.87	1.99	1.86	2.24	-0.75	0.63
28	CB6.4	2.76	2.53	3.00	2.15	1.73	2.44	-0.80	0.56
29	CB7.1N	3.73	3.73	3.77	3.04	3.04	3.08	-0.70	0.69
30	CB7.1S	2.82	2.75	3.00	2.27	2.11	2.46	-0.64	0.53
31	CB7.2	2.52	2.30	2.77	1.98	1.73	2.24	-0.57	0.53
32	CB7.2E	2.51	2.45	2.67	2.09	1.86	2.25	-0.59	0.41
33	CB7.3	2.69	2.60	3.08	2.38	2.12	2.72	-0.48	0.36
34	CB7.3E	1.42	1.22	1.52	1.21	0.74	1.30	-0.49	0.22
35	CB7.4N	1.92	1.49	2.02	1.89	0.89	2.05	-0.61	-0.02
36	CB8.1	3.28	3.26	3.58	2.61	2.45	3.05	-0.81	0.53
37	CB8.1E	3.19	3.00	3.64	2.90	2.52	3.37	-0.48	0.28
38	EE1.1	3.77	3.77	3.77	2.82	2.82	2.82	-0.95	0.95
39	EE2.1	4.26	4.26	4.27	3.19	3.19	3.20	-1.08	1.06
40	EE2.2	4.24	4.24	4.24	3.50	3.50	3.50	-0.74	0.74
41	EE3.0	7.07	7.07	7.07	3.08	3.08	3.10	-3.99	3.98
42	EE3.2	3.83	3.83	3.83	2.93	2.93	2.93	-0.90	0.90
43	EE3.4	2.72	2.72	2.81	1.77	1.77	1.85	-0.95	0.96
44	EE3.5	3.58	3.58	3.60	2.72	2.72	2.75	-0.86	0.86
45	ET2.3	5.33	5.33	5.40	5.16	5.16	5.22	-0.16	0.18

	ID	S1 MAE	S1 ME	S1 RMSE	S2 MAE	S2 ME	S2 RMSE	S2-S1 ME	S1-S2 RMSE
46	ET4.2	4.26	4.26	4.34	3.28	3.28	3.38	-0.98	0.96
47	ET5.2	4.87	4.87	4.88	2.30	2.23	2.38	-2.64	2.50
48	LE2.2	4.25	4.25	4.38	3.42	3.42	3.58	-0.83	0.80
49	LE2.3	3.70	3.70	3.79	2.81	2.80	2.92	-0.90	0.87
50	LE3.1	3.59	3.59	3.66	2.33	2.28	2.40	-1.30	1.25
51	LE3.2	3.45	3.45	3.50	2.26	2.26	2.33	-1.19	1.17
52	LE3.3	4.22	4.22	4.23	2.25	2.25	2.27	-1.97	1.96
53	LE3.4	3.32	3.32	3.34	2.19	2.19	2.22	-1.13	1.12
54	LE3.6	3.22	3.22	3.25	2.35	2.35	2.39	-0.87	0.86
55	LE3.7	3.39	3.39	3.41	2.26	2.26	2.28	-1.13	1.13
56	LE4.3	2.93	2.90	3.08	2.11	2.02	2.25	-0.87	0.83
57	LE5.3	5.75	5.75	5.93	4.28	4.28	4.51	-1.47	1.41
58	LE5.5W	4.11	4.08	4.17	3.19	3.07	3.30	-1.01	0.88
59	RET2.4	5.32	5.32	5.50	4.48	4.47	4.67	-0.85	0.84
60	WE4.1	2.30	2.30	2.32	1.32	1.32	1.35	-0.98	0.97
61	WE4.2	2.96	2.92	2.98	2.06	2.00	2.10	-0.92	0.88
62	WE4.3	2.81	2.81	2.82	1.63	1.62	1.65	-1.19	1.17
63	WE4.4	3.01	3.01	3.02	1.55	1.55	1.56	-1.46	1.46
64	WT5.1	2.15	1.12	2.34	1.75	0.22	2.04	-0.91	0.30
	Avg	3.81	3.76	3.94	2.95	2.85	3.09	-0.91	0.85
	Stdev	1.32	1.38	1.33	1.20	1.29	1.21	0.56	0.57

Figure 8 shows 2016 salinity profile plots for station EE3.0 at 11 times throughout the year. The Scenario 2 outputs at EE3.0 are closer to observations than Scenario 1 outputs. This station is located in Fishing Bay and relatively near the outflows of the Nanticoke and Wicomico Rivers (see reference map in the lower right of Figure 8). Very little salinity stratification is observed or simulated at this location. Further illustrated by numerous observed salinity profiles in Appendix B, low stratification is not uncommon for locations in shallower portions of the Bay where the water is well mixed. At EE3.0 observed values are available to 6-m while simulated values are only available to 4-m. These differences could be due to inaccurate CBOFS2 bathymetry. It is well known that bathymetry is a key input to achieve accurate shallow water hydrodynamic modeling and Ye et al. (2018) illustrate the importance of accurate bathymetry in Chesapeake Bay modeling. Bathymetry errors, particularly in shallow portions of the Bay, could have a substantial impact on the results we are presenting here. However, it is beyond the scope of this work to explicitly assess multiple sources of error beyond freshwater changes on the modeling.

Figure 9 shows observed and simulated profile plots at the CB5.2 observation station, which is located in deeper water near the center of the Bay. Here, away from the influence of local tributaries, the differences between Scenario 1 and Scenario 2 are much smaller. More stratification with depth is also observed at this location compared to EE3.0 because freshwater is not fully mixing in deeper portions of the Bay.

In Figure 10, salinity profiles for station LE3.1 show moderate effects of the freshwater inflow changes from Scenario 1 to Scenario 2. The impacts are somewhere in between the small estuary station (EE3.0) and the mid-Bay station (CB5.2).

For the same stations assessed in Figures 8-10, Figures 11a-c show time series of simulated and observed salinity at a 1-m depth (left axis) along with time series of river inflows (right axis). Out of all 64 stations in this study, EE3.0 saw the biggest average RMSE improvement of about 4 psu from Scenario 1 to 2 (Figure 7 and Table 3). The salinity time series in Figure 11a reflect this average improvement. The local inflow time series in Figure 11a, which are the sum of the Nanticoke and Wicomico simulations, indicate why the salinity simulations are so much different. Although the CBOFS2 baseline (Scenario 1) includes an inflow node near the Nanticoke outlet, it does not use any gauges from the Nanticoke or Wicomico Rivers to derive inflow estimates, yielding inflow estimates that are far too low at the Nanticoke node. Scenario 2 corrects this problem.

Figure 11b plots salinity and flow time series for CB5.2, which is located in the middle of the Bay. The flow traces in 11b include the totals from all tributaries. As at EE3.0, sudden drops in salinity are associated with large freshwater events, affirming the importance of river inflows on salinity distribution throughout the Bay. Not surprisingly, the difference between Scenarios 1 and 2 is not as large at CB5.2, closer to the center of the Bay. At the 1-m depth shown here, the improvement in salinity mean absolute error (MAE) from Scenario 1 to 2 (S1-S2) is 4.0 psu for EE3.0 but only 0.7 psu for CB5.2.

Figure 11c is for LE3.1 located near the outlet of the Rappahannock River. The inflows in Figure 11c are for the Rappahannock. Scenario 2 includes more inflow and produces lower salinity simulations as expected. The Scenario 2 salinity at 1-m drops closer to the observations, not as dramatically as at location EE3.0, but more so than at CB5.2. The MAE improvement from S1 to S2 is 1.3 psu for station LE3.1.

Although Scenario 2 consistently improves the salinity predictions over Scenario 1, it does not completely eliminate the high bias from the simulations at most locations (see Figures 6c and d as well as Figures 11a-c). Despite the remaining bias, the CBOFS2 model does show a consistent temporal correlation with observations in Figures 11a-c as well as at other locations (see Appendix C for other locations).

Figure 7c shows one location, CB1.1, where the Scenario 2 salinity error was slightly higher than the Scenario 1 error in terms of RMSE. CB1.1 is located at the mouth of the Susquehanna River. Figure 12 shows that observed and simulated salinities for this site during much of 2016 are close to zero. However, in the low flow period from September through November 2016, Scenario 2 simulates some non-zero salinity values at the 1-m depth in the range of 0 to 3 psu. During this time period, Scenario 1 simulates lower salinities close to 0. Scenario 1 simulations are closer to observations, which include only one non-zero observation during this period, 0.09 psu on 10/19/2016. Flow data for the Susquehanna River at Conowingo Dam from the USGS are plotted along with the Scenario 1 and 2 Susquehanna inflows in Figure 12. These data indicate that the Susquehanna flows fed to the CBOFS2 operational model (Scenario 1) were too high during September and October of 2016. The reason for this erroneous inflow is unknown. Because the erroneous, higher flows in Scenario 1 actually yield a better salinity simulation at CB1.1, this suggests that sources of model error other than streamflow are causing the salinity

over-estimates in Scenario 2.

We selected the sites in Figures 8-12 to highlight different types of locations within the Bay. This included a relatively shallow location near the edge of the Bay where the local river flows have a relatively large influence (EE3.0), a station near the main channel of the Bay (CB5.2), a station near the outlet of a medium size river (LE3.1), and a station near the outlet of a major river (CB1.1). Graphics and tabular results for all 64 observation stations and both the 2005 and 2016 simulation periods are also available to further support our conclusions. These details are provided in Appendices A, B, and C due to their considerable length.

Out of the 64 stations analyzed in the 2016 period, the average profile mean error (ME) improved by 0-1 psu in 44 stations, 1-2 psu at 17 stations, 2-3 psu at 1 station, and 4 psu at 1 station (Table 3, Figure 6f). The average profile ME increased by 0.4 psu for one station (CB1.1) for reasons explained above. As expected, we see greater improvements in shallower waters near tributary inflows.

While we see strong evidence of salinity simulation improvements from more accurate river inflows, there is still an overall salinity bias in Scenario 2. From Table 3, the ME over all observing stations dropped from 3.76 to 2.85 psu for the 2016 period, a modest improvement. Lanerolle et al. (2016) note that this improved level of salinity accuracy would not be adequate for applications such as Vibrio forecasting, citing accuracy requirements for CBOFS as +/-1 psu and +/-1 degree C. To achieve results closer to these values for Vibrio forecasting, Lanerolle et al. (2016) statistically post-process the CBOFS2 output. This would still be recommended with the improved freshwater inflows we demonstrate here.

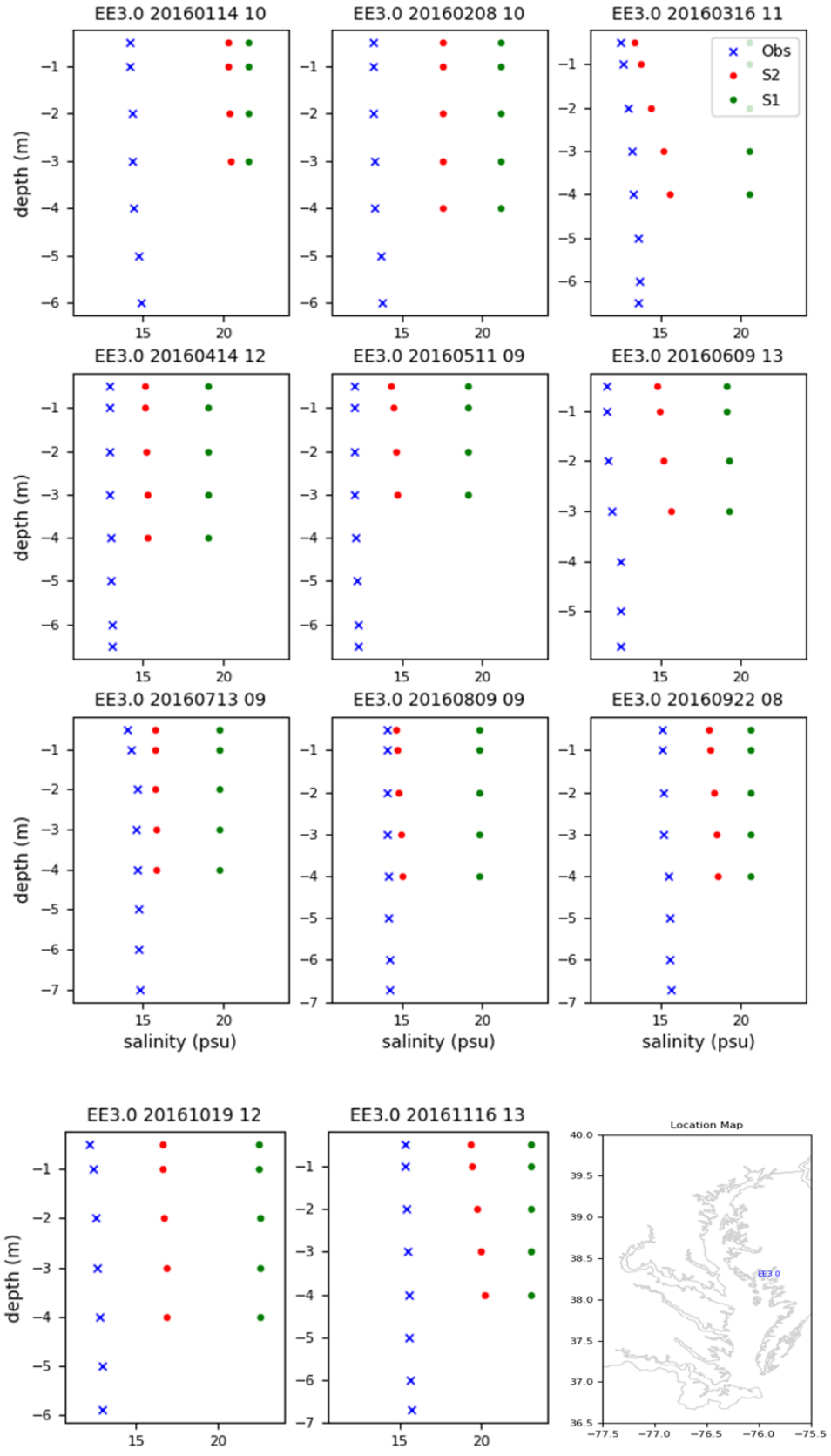

Figure 8. Salinity profile plots for all observation dates in the 2016 simulation period at location EE3.0.

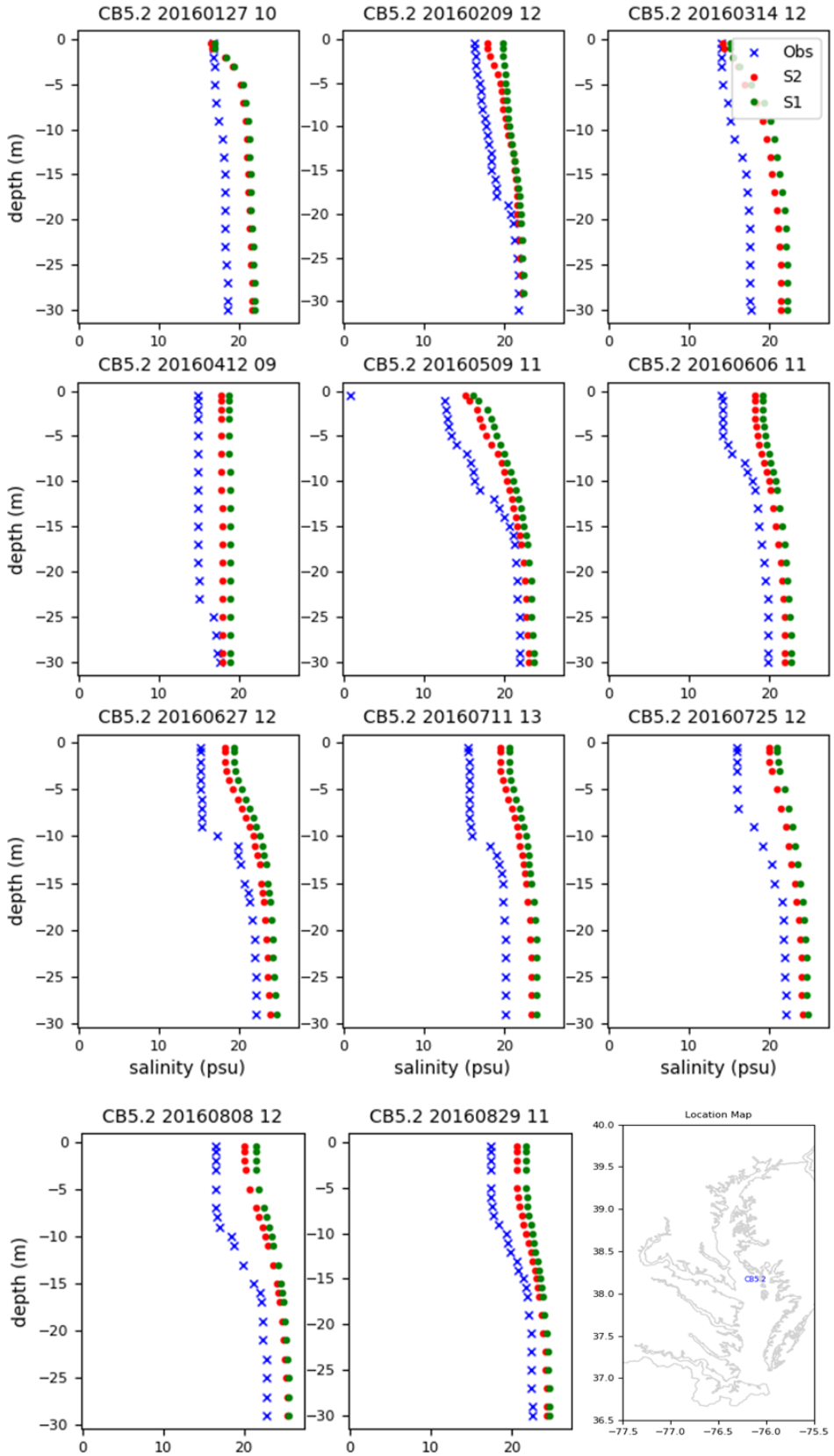

Figure 9. Salinity profile plots for all observation dates in the 2016 simulation period at location CB5.2.

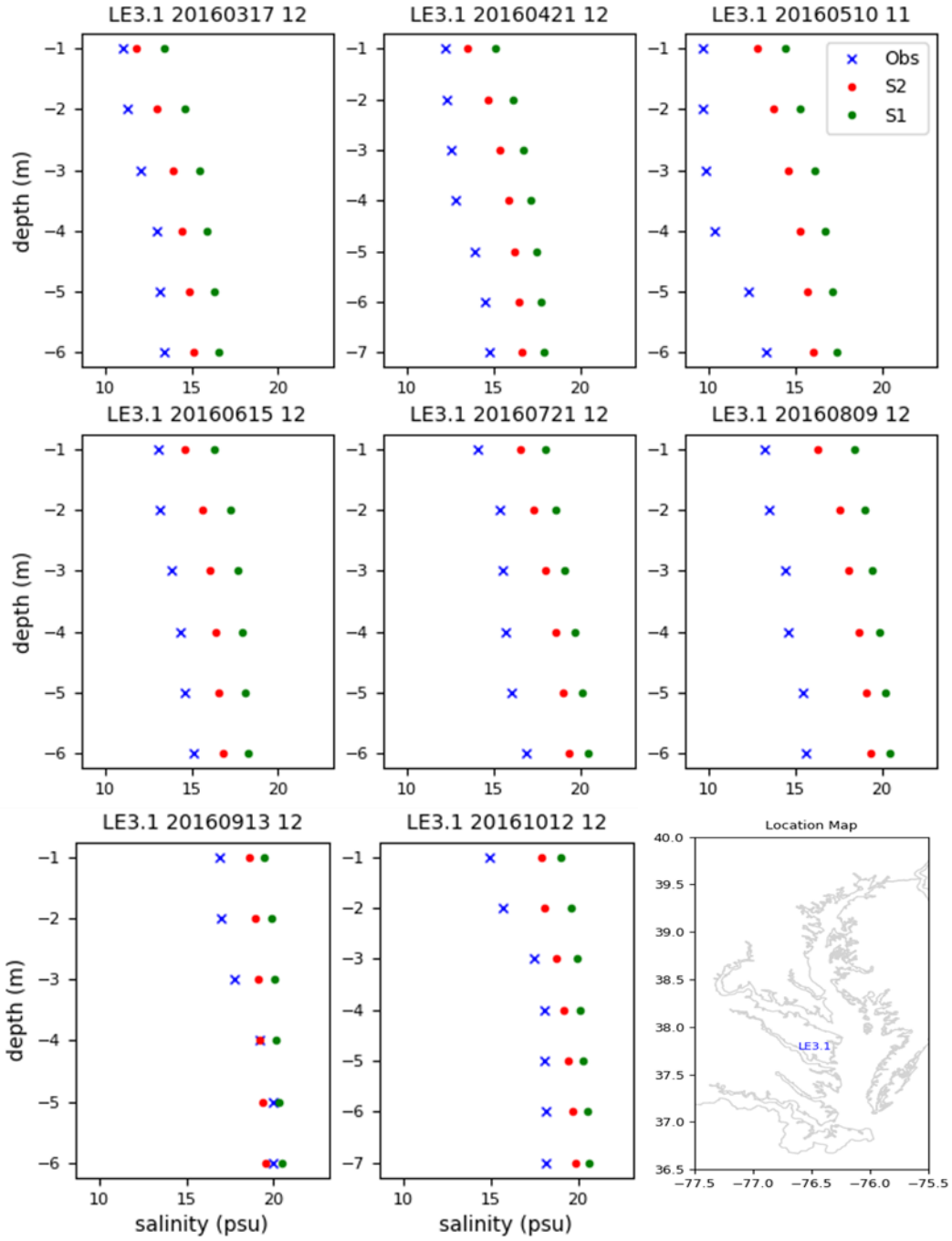

Figure 10. Salinity profile plots for all observation dates in the 2016 simulation period at location LE 3.1.

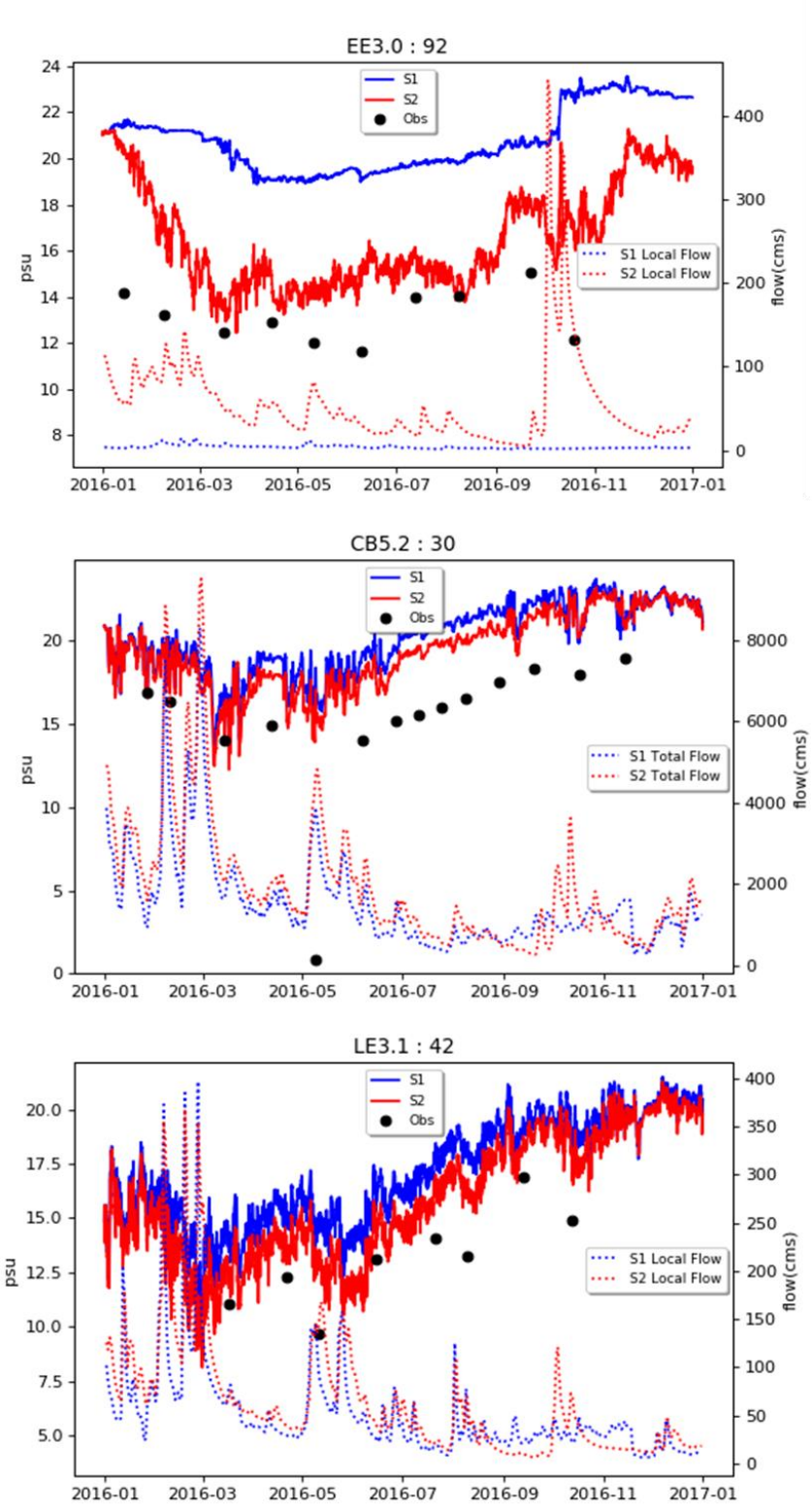

Figure 11. Simulated salinity from Scenarios 1 and 2 along with discrete observations at 1-m depth and relevant inflows. (a) EE3.0 with inflows from the nearby Nanticoke and Wicomico Rivers, (b) CB5.2 with inflows from all tributaries, (c) LE3.1 with inflows from the Rappahannock River.

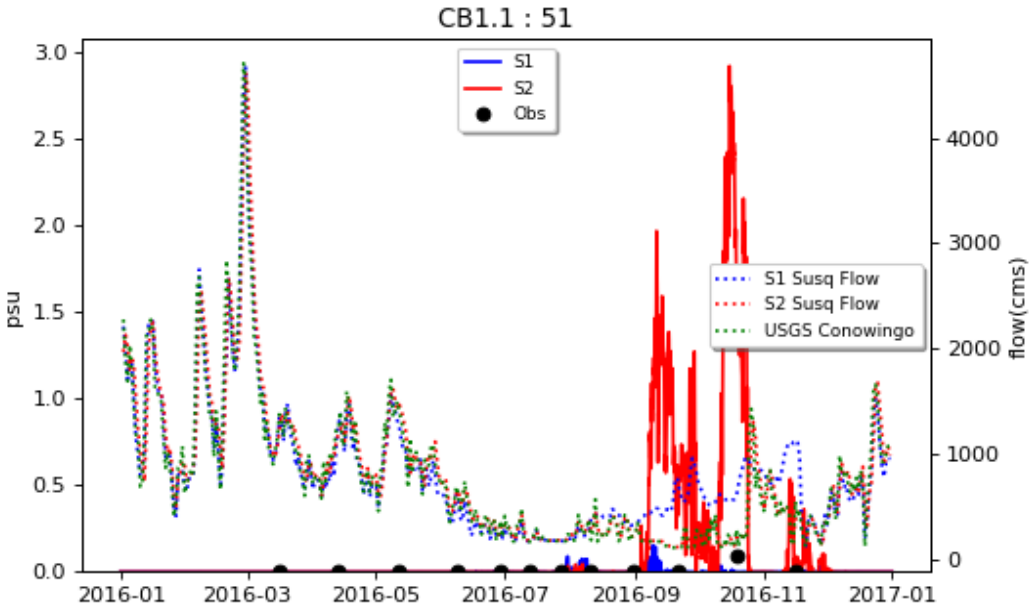

Figure 12. Simulated salinity from Scenarios 1 and 2 along with discrete observations at 1-m depth. Station CB1.1 is at the mouth of the Susquehanna R. Simulated and observed salinity are zero except during low flow periods. S1, S2, and USGS observed flows below Conowingo Dam are shown.

Conclusions and Recommendations for Future Work

Increasing the number of inflow nodes in CBOFS2 from 13 to 60 and explicit hydrologic modeling of an additional 16% percent of the land area improve salinity simulations. Lower mean errors (a.k.a. bias) and lower root mean squared error (RMSE) confirm this when comparing simulations to observations at 64 sampling sites. Spatial trends in the results are consistent with expectations. That is, greater improvements are seen from Scenario 1 to 2 at sampling sites in shallower water and near river inflows that are not modeled in Scenario 1.

In our Scenario 2 simulations, we used observed inflows for 79% of the Chesapeake drainage and model simulations for an additional 16% of the area. The accuracy of the watershed modeling in added areas is limited in part because the gridded hydrologic model is uncalibrated. In addition, this study was limited to simulations, without considering the additional errors that would be introduced in a forecast period driven by precipitation forecasts rather than observed precipitation. Nonetheless, our results show that additional work to implement more detailed hydrologic modeling in the NOAA operational forecast environment is likely to produce benefits. Our CBOFS2 simulations with 60 nodes ran smoothly without numerical stability problems.

A reasonable next step towards operational implementation and to assess results in forecast mode would be to run a CBOFS2 60 inflow configuration with live data in parallel to the current operational model. Our configuration has been provided to NOS COOPs for possible use in this manner.

The most practical source of inflows for ungaged rivers in a real-time configuration would be the National Water Model (NWM). For reasons explained above, we used the HL-RDHM model in this study. For small, ungaged basins, we would expect NWM and HL-RDHM forecasts to be relatively comparable, although more analysis of this would be prudent. Long period simulations for NWM at all 60 locations of interest were not available for this study.

For forecasts at inflow nodes associated with larger rivers, such as the Susquehanna, Potomac, James, we would recommend using the official RFC model forecasts where available, rather than NWM, because they are known to be substantially more accurate. As evidence of this, Figure 13 shows a comparison of the 3-day average RMSE calculated from all 12 UTC medium-range NWM v2.0 forecasts and 12 UTC RFC operational forecasts from July 1, 2019 to April 30, 2020. Figure 13a includes data for 62 gaged headwater basins (approximately 300 mi^2 in size) where MARFC has been tracking NWM performance, as well forecasts for the largest rivers flowing to the Bay. NWM forecasts for the three largest Chesapeake Rivers have a substantially higher RMSE than the RFC forecasts (Figure 13a). For smaller basins, while NWM forecast errors still tend to be higher, the differences represent considerably less volume than differences for the three largest rivers. Regardless, outside of the major rivers, the RFC model forecasts are not available for the 60 local watersheds we modeled in Scenario 2, so NWM is the best available option for these locations. With this approach, initial application of NWM would only be in about 16% of the modeled area, capturing the dynamics in these smaller tributaries while avoiding the larger volume errors seen on larger rivers. With the resolution of NWM and some additional testing, future implementations could also increase the number of connecting nodes beyond 60.

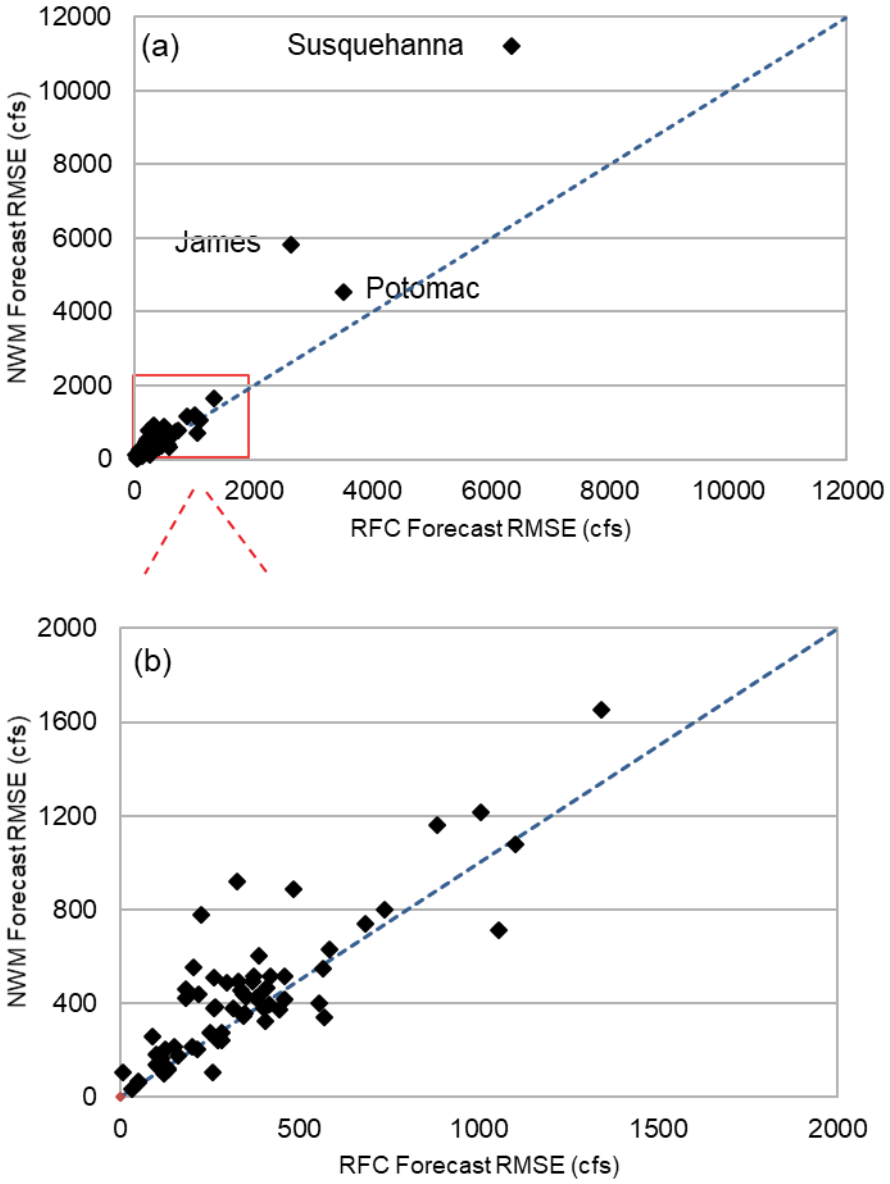

Figure 13. 3-day average RMSE calculated for NWM and RFC operational forecasts at 62 headwater basins plus the outlets of four major tributaries (Susquehanna, Potomac, Rappahannock, and James): (a) all locations, and (b) all but the three largest basins.

Acknowledgments

Thank you to Lyon Lanerolle (formerly NOS), who provided the CBOFS2 program, data, and guidance necessary to get this project started at MARFC where we had no prior CBOFS2 experience. Thank you also to Aijun Zhang, Zizang Yang, and Machuan Peng who provided guidance and data to set up the 2016 simulations and answered additional questions about CBOFS2. In addition, thanks to NOAAs North Atlantic Regional Team for providing student funding, and the NOAA Chesapeake Bay Office and Chesapeake Research Consortium for

helping to facilitate the student internships for three summers.

References

Chesapeake Bay Program (CBP), 2020: Chesapeake Bay Program (CBP) Water Quality Database (1984-Present), Accessed June 2017, https://www.chesapeakebay.net/what/downloads/cbp_water_quality_database_1984_present.

Cerco, C., S.-C. Kim, and M. Noel, 2010: The 2010 Chesapeake Bay Eutrophication Model – A Report to the US Environmental Protection Agency Chesapeake Bay Program and to The US Army Engineer Baltimore District, US Army Engineer Research and Development Center, Vicksburg, MS.

Feng, Y., M.A.M. Friedrichs, J. Wilkin, H. Tian, Q. Yang, E. E. Hofmann, J.D. Wiggert, and R.R. Hood, 2015. Chesapeake Bay nitrogen fluxes derived from a land-estuarine ocean biogeochemical modeling system: Model description, evaluation, and nitrogen budgets, J. of Geophys. Res.- Biogeosciences, 120, https://doi.org/10.1002/2015JG002931.

Koren, V., S. Reed, M. Smith, Z. Zhang, and D.J. Seo, 2004. Hydrology laboratory research modeling system (HLRMS) of the US national weather service, Journal of Hydrology, 291(3–4), 297–318, https://doi.org/10.1016/j.jhydrol.2003.12.039.

Koren, V., M. Smith, Z. Cui, and B. Cosgrove 2007: Physically-based Modifications to the Sacramento Soil Moisture Accounting Model: Modeling the Effects of Frozen Ground on the Rainfall-Runoff Process, *NOAA Technical Report NWS 52*, 43 pp.

Lanerolle, L., R. Patchen, and F. Aikman III, 2011: The Second Generation Chesapeake Bay Operational Forecast System (CBOFS2): Model Development and Skill Assessment, *NOAA Technical Report NOS CS 29*, Coast Survey Development Laboratory, Silver Spring, MD, 77 pp.

Lanerolle, L., R. Daniels, B. Zhang, and J. Jacobs, 2016: Skill assessment of NOAAs Chesapeake Bay Vibrio vulnificus model, NOAA Technical Memorandum NOS NCCOS 215, NOAA National Centers for Coastal Ocean Science, Center for Coastal Environmental Health and Biomolecular Research, Cooperative Oxford Laboratory, Oxford, MD. 18 pp., https://doi.org/10.7289/V5/TM-NOS-NCCOS-215.

Conkright, M.E., R.A. Locarnini, H.E. Garcia, T.D. O'Brian, T.P. Boyer, C. Stephens, and J.I. Anotonov, 2002. World Ocean Atlas 2001: Objective Analysis, Data Statistics, and Figures, CD-ROM Documentation, National Oceanographic Data Center, Silver Spring, MD, 17 pp.

Li, Z., T.F. Gross, W.B. Brown, H.V. Wang, R.H. Hood, 2001: A Near Real Time Simulation of Salinity, Temperature and Sea Nettles (Chrysaora quinquecirrha) in Chesapeake Bay, ASCE *Estuarine and Coastal Modeling*, 467 – 478, ASCE, New York.

Mesinger, F., and Coauthors, 2006: North American Regional Reanalysis. *Bull. Amer. Meteor*. Soc., 87(3), 343–360.

Mizukami, N., and V. Koren, 2008: Methodology and Evaluation of Melt Factor Parameterization for Distributed Snow-17, Oral Presentation, AGU Fall Meeting, December 2008, San Francisco.

National Centers for Coastal Ocean Science (NCCOS), 2017: Vibrio Predictive Models, Accessed May 2020, https://products.coastalscience.noaa.gov/vibrioforecast/chesapeake/default.aspx.

Office of Water Prediction, 2020: National Water Model (NWM), Accessed September 2020, https://water.noaa.gov/about/nwm.

NOAA National Ocean Service, 2011: Chesapeake Bay Operational Forecast System, Accessed May 2020, https://tidesandcurrents.noaa.gov/ofs/publications/CBOFS_Onepager.pdf.

NOAA, Dec. 2016: NOAA Water Initiative, Vision and Five-Year Plan, Accessed September 2020, https://www.noaa.gov/water/explainers/noaa-water-initiative-vision-and-five-year-plan.

NOAA Ocean Prediction Center (OPC), 2019: Sea Nettles Probability of Encounters, Accessed May 2020, https://ocean.weather.gov/Loops/SeaNettles/prob/SeaNettles.php.

Reed, S., V. Koren, M. Smith, Z. Zhang, F. Moreda, D.J. Seo, and DMIP Participants, 2004: Overall distributed model intercomparison project results, *Journal of Hydrology*, **298**, 27-60.

Smith, M.B., V. Koren, Z. Zhang, Y. Zhang, S. Reed, Z. Cui, F. Moreda, B. Cosgrove, N. Mizukami, E. Anderson, and DMIP 2 Participants, 2012: Results of the DMIP 2 Oklahoma experiments, *Journal of Hydrology*, 418-419, 17-48, https://doi.org/10.1016/j.jhydrol.2011.08.056.

Xu, J., W. Long, J. Wiggert, L. Lanerolle, C. Brown, R. Murtugudde, and R. Hood, 2012: Climate Forcing and Salinity Variability in Chesapeake Bay, USA, *Estuaries and Coasts*, **35**, 237-261, https://doi.org/10.1007/s12237-011-9423-5.

Ye, F., Y. Zhang, H. Wang, M.A. Friedrichs, I. Irby, E. Alteljevich, A. Valle-Levinson, Z. Wang, H. Huang, J. Shen, and J. Du, 2018: A 3D unstructured-grid model for the Chesapeake Bay: Importance of bathymetry, *Ocean Modelling*, **127**, 16-39.

Appendices

Appendix A. Tabular results for 2004 period.

Appendix B. Simulated and observed profile plots for all times and locations.

1. 2004 (212 pages)
2. 2016 (114 pages)

Appendix C. Simulated and observed time-series plots for all locations.

1. 2004 (8 pages)
2. 2016 (8 pages)

(CONTINUED FROM FRONT COVER)

NWS ER 46 An Objective Method of Forecasting Summertime Thunderstorms. John F. Townsend and Russell J. Younkin. May 1972. (COM-72-10765).

NWS ER 47 An Objective Method of Preparing Cloud Cover Forecasts. James R. Sims. August 1972. (COM-72-11382).

NWS ER 48 Accuracy of Automated Temperature Forecasts for Philadelphia as Related to Sky Condition and Wind Direction. Robert B. Wassall. September 1972. (COM-72-11473).

NWS ER 49 A Procedure for Improving National Meteorological Center Objective Precipitation Forecasts. Joseph A. Ronco, Jr. November 1972. (COM-73-10132).

NWS ER 50 PEATMOS Probability of Precipitation Forecasts as an Aid in Predicting Precipitation Amounts. Stanley E. Wasserman. December 1972. (COM-73-10243).

NWS ER 51 Frequency and Intensity of Freezing Rain/Drizzle in Ohio. Marvin E. Miller. February 1973. (COM-73-10570).

NWS ER 52 Forecast and Warning Utilization of Radar Remote Facsimile Data. Robert E. Hamilton. July 1973. (COM-73-11275).

NWS ER 53 Summary of 1969 and 1970 Public Severe Thunderstorm and Tornado Watches Within the National Weather Service, Eastern Region. Marvin E. Miller and Lewis H. Ramey. October 1973. (COM-74-10160)

NWS ER 54 A Procedure for Improving National Meteorological Center Objective Precipitation Forecasts - Winter Season. Joseph A. Ronco, Jr. November 1973. (COM-74-10200).

NWS ER 55 Cause and Prediction of Beach Erosion. Stanley E. Wasserman and David B. Gilhousen. December 1973.(COM-7410036).

NWS ER 56 Biometeorological Factors Affecting the Development and Spread of Planet Diseases. V.J. Valli. July 1974. (COM-74-11625/AS).

NWS ER 57 Heavy Fall and Winter Rain In The Carolina Mountains. David B. Gilhousen. October 1974. (COM-74-11761/AS).

NWS ER 58 An Analysis of Forecasters' Propensities In Maximum/Minimum Temperature Forecasts. I. Randy Racer. November 1974. COM-75-10063/AS).

NWS ER 59 Digital Radar Data and its Application in Flash Flood Potential. David D. Sisk. March 1975. (COM-75-10582/AS).

NWS ER 60 Use of Radar Information in Determining Flash Flood Potential. Stanley E. Wasserman. December 1975. (PB250071/AS).

NWS ER 61 Improving Short-Range Precipitation Guidance During the Summer Months. David B. Gilhousen. March 1976. (PB256427).

NWS ER 62 Locally Heavy Snow Downwind from Cooling Towers. Reese E. Otts. December 1976. (PB263390/AS).

NWS ER 63 Snow in West Virginia. Marvin E. Miller. January 1977. (PB265419/AS).

NWS ER 64 Wind Forecasting for the Monongahela National Forest. Donald E. Risher. August 1977. (PB272138/AS).

NWS ER 65 A Procedure for Spraying Spruce Budworms in Maine during Stable Wind Conditions. Monte Glovinsky. May 1980. (PB80-203243).

NWS ER 66 Contributing Factors to the 1980-81 Water Supply Drought, Northeast U.S. Solomon G. Summer. June 1981. (PB82-172974).

NWS ER 67 A Computer Calculation and Display System for SLOSH Hurricane Surge Model Data. John F. Townsend. May 1984. (PB84-198753).

NWS ER 68 A Comparison Among Various Thermodynamic Parameters for the Prediction of Convective Activity. Hugh M. Stone. April 1985. (PB85-206217/AS).

NWS ER 69 A Comparison Among Various Thermodynamic Parameters for the Prediction of Convective Activity, Part II. Hugh M. Stone. December 1985. (PB86-142353/AS).

NWS ER 70 Hurricane Gloria's Potential Storm Surge. Anthony G. Gigi and David A. Wert. July 1986. (PB86-226644/AS).

NWS ER 71 Washington Metropolitan Wind Study 1981-1986. Clarence Burke, Jr. and Carl C. Ewald. February 1987. (PB87-151908/AS).

NWS ER 72 Mesoscale Forecasting Topics. Hugh M. Stone. March 1987. (PB87-180246/AS).

NWS ER 73 A Procedure for Improving First Period Model Output Statistics Precipitation Forecasts. Antonio J. Lacroix and Joseph A. Ronco. Jr. April 1987. (PB87-180238/AS).

NWS ER 74 The Climatology of Lake Erie's South Shoreline. John Kwiatkowski. June 1987. (PB87-205514/AS).

NWS ER 75 Wind Shear as a Predictor of Severe Weather for the Eastern United States. Hugh M. Stone. January 1988. (PB88-157144).

NWS ER 76 Is There A Temperature Relationship Between Autumn and the Following Winter? Anthony Gigi. February 1988. (PB88-173224).

NWS ER 77 River Stage Data for South Carolina. Clara Cillentine. April 1988. (PB88-201991/AS).

NWS ER 78 National Weather Service Philadelphia Forecast Office 1987 NOAA Weather Radio Survey & Questionnaire. Robert P. Wanton. October 1988. (PB89-111785/AS).

NWS ER 79 An Examination of NGM Low Level Temperature. Joseph A. Ronco, Jr. November 1988. (PB89- 122543/AS).

NWS ER 80 Relationship of Wind Shear, Buoyancy, and Radar Tops to Severe Weather 1988. Hugh M. Stone. November 1988. (PB89-1222419/AS).

NWS ER 81 Relation of Wind Field and Buoyancy to Rainfall Inferred from Radar. Hugh M. Stone. April 1989. (PB89-208326/AS).

NWS ER 82 Second National Winter Weather Workshop, 26-30 Sept. 1988: Postprints. Laurence G. Lee. June 1989.(PB90147414/AS).

NWS ER 83 A Historical Account of Tropical Cyclones that Have Impacted North Carolina Since 1586. James D. Stevenson. July 1990. (PB90-259201).

NWS ER 84 A Seasonal Analysis of the Performance of the Probability of Precipitation Type Guidance System. George J. Maglaras and Barry S. Goldsmith. September 1990. (PB93-160802)

NWS ER 85 The Use of ADAP to Examine Warm and Quasi-Stationary Frontal Events in the Northeastern United States. David R. Vallee. July 1991. (PB91-225037)

NWS ER 86 Rhode Island Hurricanes and Tropical Storms A Fifty-Six Year Summary 1936-1991. David R. Vallee. March 1993. (PB93-162006)

NWS ER 87 Post-print Volume, Third National Heavy Precipitation Workshop, 16-20 Nov. 1992. April 1993. (PB93-186625)

NWS ER 88 A Synoptic and Mesoscale Examination of the Northern New England Winter Storm of 29-30 January 1990. Robert A. Marine and Steven J. Capriola. July 1994. (PB94-209426)

NWS ER 89 An Initial Comparison of Manual and Automated Surface Observing System Observations at the Atlantic City, New Jersey, International Airport. James C. Hayes and Stephan C. Kuhl. January 1995.

NWS ER 90 Numerical Simulation Studies of the Mesoscale Environment Conducive to the Raleigh Tornado. Michael L. Kaplan, Robert A. Rozumalski, Ronald P. Weglarz, Yuh-Lang Lin , Steven Businger, and Rodney F. Gonski. November 1995.

NWS ER 91 A Climatology of Non-convective High Wind Events in Western New York State. Thomas A. Niziol and Thomas J. Paone. April 2000.

NWS ER 92 Tropical Cyclones Affecting North Carolina Since 1586 - An Historical Perspective. James E. Hudgins. April 2000.

NWS ER 93 A Severe Weather Climatology for the Wilmington, NC WFO County Warning Area. Carl R., Morgan. October 2001.

NWS ER 94 Surface-based Rain, Wind, and Pressure Fields in Tropical Cyclones over North Carolina since 1989. Joel Cline. June 2002.

NWS ER 95 A Severe Weather Climatology for the Charleston, South Carolina, WFO County Warning Area. Stephen Brueske, Lauren Plourd, Matthen Volkmer. July 2002.

NWS ER 96 A Severe Weather Climatology for the WFO Wakefield, VA County Warning Area. Brian T. Cullen. May 2003. (PB2003-105462)

NWS ER 97 Severe Weather Climatology for the Columbia, SC WFO County Warning Area. Leonard C. Vaughan. September 2003. (PB2004-100999)

NWS ER 98 Climatology of Heavy Rainfall Associated with Tropical Cyclones Affecting the Central Appalachians. James Hudgins, Steve Keighton, Kenneth Kostura, Jan Jackson. September 2005.

NWS ER 99 A Severe Weather Climatology for the WFO Blacksburg, Virginia, County Warning Area. Robert Stonefield, James Hudgins. January 2007.

NWS ER 100 Tropical Cyclones Affecting North Carolina Since 1586 - An Historical Perspective. James E. Hudgins. October 2007.

NWS ER 101 A Severe Weather Climatology for the Raleigh, NC County Warning Area. Clyde Brandon Locklear. May 2008.

NWS ER 102 A Severe Weather Climatology for the Wilmington, OH County Warning Area (1950-2004). Michael D. Ryan. May 2008.

NWS ER 103 A Climatology of Flash Flood Events for the National Weather Service Eastern Region, Alan M. Cope. June 2009.

NWS ER 104 An Abbreviated Flash Flood/Flood Climatology (1994-2007) for the WFO Blacksburg, VA County Warning Area., Robert Stonefield and Jan Jackson. September 2009.

NWS ER 105 Dense Fog Climatology for the Blue Ridge Foothills and Piedmont Areas of the Blacksburg, VA County Warning Area for the Period 1973-2008. Jan Jackson, Ken Kostura and William Perry. February 2011.

NWS ER 106 Climatology of Storm Data Events for the NWS Mount Holly Forecast Area, Alan M. Cope. March 2016.

NOAA SCIENTIFIC AND TECHNICAL PUBLICATIONS

The National Oceanic and Atmospheric Administration was established as part of the Department of Commerce on October 3, 1970. The mission responsibilities of NOAA are to assess the socioeconomic impact of natural and technological changes in the environment and to monitor and predict the state of the solid Earth, the oceans and their living resources, the atmosphere, and the space environment of the Earth.

The major components of NOAA regularly produce various types of scientific and technical information in the following kinds of publications:

PROFESSIONAL PAPERS--Important definitive research results, major techniques, and special investigations.

CONTRACT AND GRANT REPORTS--Reports prepared by contractors or grantees under NOAA sponsorship.

ATLAS--Presentation of analyzed data generally in the form of maps showing distribution of rainfall, chemical and physical conditions of oceans and atmosphere, distribution of fishes and marine mammals, ionospheric conditions, etc.

TECHNICAL SERVICE PUBLICATIONS--Reports containing data, observations, instructions, etc. A partial listing includes data serials; prediction and outlook periodicals; technical manuals, training papers, planning reports, and information serials; and miscellaneous technical publications.

TECHNICAL REPORTS--Journal quality with extensive details, mathematical developments, or data listings.

TECHNICAL MEMORANDUMS--Reports of preliminary, partial, or negative research or technology results, interim instructions, and the like.

.

Information on availability of NOAA publications can be obtained from:

NATIONAL TECHNICAL INFORMATION SERVICE
U.S. DEPARTMENT OF COMMERCE
5285 PORT ROYAL ROAD SPRINGFIELD, VA 22161